Helsinki University of Technology
Materials Physics Laboratory
Espoo 2003

DESIGN AND APPLICATIONS OF OPTICAL MICROSPHERE RESONATORS

Juha-Pekka Laine

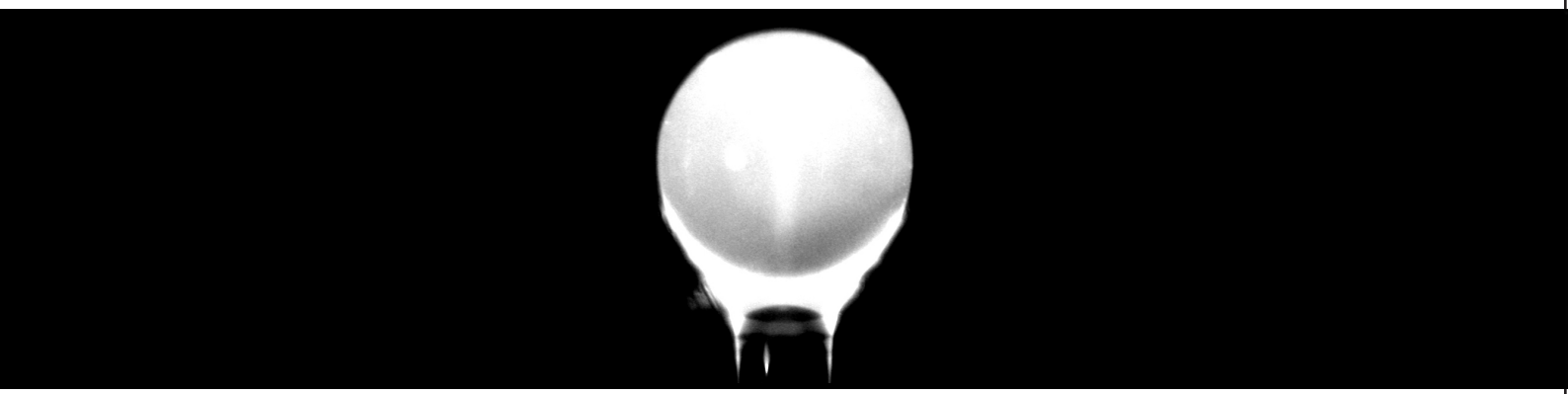

TEKNILLINEN KORKEAKOULU
TEKNISKA HÖGSKOLAN
HELSINKI UNIVERSITY OF TECHNOLOGY
TECHNISCHE UNIVERSITÄT HELSINKI
UNIVERSITE DE TECHNOLOGIE D'HELSINKI

Helsinki University of Technology Publications in Engineering Physics

Teknillisen korkeakoulun teknillisen fysiikan julkaisuja

Espoo 2003 TKK-F-A821

DESIGN AND APPLICATIONS OF OPTICAL MICROSPHERE RESONATORS

Juha-Pekka Laine

Dissertation for the degree of Doctor of Science in Technology to be presented with due permission for public examination and debate in Auditorium F1 at Helsinki University of Technology (Espoo, Finland) on the 22nd of April, 2003, at 12 o'clock noon.

Helsinki University of Technology
Department of Engineering Physics and Mathematics
Materials Physics Laboratory

Teknillinen korkeakoulu
Teknillisen fysiikan ja matematiikan osasto
Materiaalifysiikan laboratorio

Distribution:
Helsinki University of Technology
Materials Physics Laboratory
P.O. Box 2200
FIN-02015 HUT
Tel. +358-9-451-3168
Fax. +358-9-451-3164
E-mail: jpl@focus.hut.fi

ISBN 951-22-6447-1 (printed)
ISBN 951-22-6448-X (pdf)
ISSN 1456-3320

Otamedia Oy
Espoo 2003

HELSINKI UNIVERSITY OF TECHNOLOGY
P.O. BOX 1000, FIN-02015 HUT
http://www.hut.fi

ABSTRACT OF DOCTORAL DISSERTATION

Author Juha-Pekka Jaakko Valtteri Laine

Name of the dissertation

Design and applications of optical microsphere resonators

Date of manuscript 24.9.2002 | Date of the dissertation 22.4.2003

☐ Monograph ☑ Article dissertation (summary + original articles)

Department Engineering Physics and Mathematics
Laboratory Materials Physics Laboratory
Field of research High-Q optical resonators
Opponent(s) Prof. Richard K. Chang, Yale University, New Haven, CT, U.S.A.
Supervisor Prof. Martti M. Salomaa, Helsinki University of Technology, Espoo, Finland
(Instructor) Prof. Hermann A. Haus, Massachusetts Institute of Technology, Cambridge, MA, U.S.A.

Abstract

Microscopic spherical silica particles, as small as 0.1 mm in diameter, can function as optical whispering-gallery-mode resonators supporting Q-values of 10^8 and beyond. Such enormously high quality factors represent unique performance characteristics: an extremely narrow resonant linewidth, long decay time and a high energy density. Envisioned uses for these miniature high-Q resonators include, for example, cavity-QED experimentation, detection and sensing, frequency stabilization, and optical filtering functions.

Until recently, the primary obstacle discouraging applications-oriented development of microsphere resonators has been the fundamental novelty of the various fabrication and handling processes involved – especially in the construction of the advanced optical couplers necessary for efficient sphere mode excitation. In this thesis, novel coupler designs and fabrication methods are presented. New microsphere resonator applications are demonstrated as well, including a narrow-band wavelength-drop device and an acceleration sensor. The most important invention is the antiresonant waveguide coupler, SPARROW, which allows inexpensive and consistent wafer-based fabrication of very efficient microsphere coupling tools.

Keywords microsphere, optical resonator, whispering-gallery mode

UDC | Number of pages 56
ISBN (printed) 951-22-6447-1 | ISBN (pdf) 951-22-6448-X
ISBN (others) | ISSN 1456-3320
Publisher Helsinki University of Technology, Materials Physics Laboratory
Print distribution
☑ The dissertation can be read at http://lib.hut.fi/Diss/

Preface

The work described in this doctoral thesis was performed in the Research Laboratory of Electronics, Massachusetts Institute of Technology, and at the Charles Stark Draper Laboratory mainly over the 1998-2001 timeframe.

First and foremost, I would like to extend heartfelt thanks to Professor Martti Salomaa for his continuous strong backing and encouragement during the length of this doctoral program.

I am greatly indebted to M.I.T. Institute Professor Hermann Haus for the wonderful opportunity to work in his research group. I thank Professor Haus for providing invaluable insights and advice over the years, as well as for demonstrating an unending supply of patience with this junior scientist.

My expressions of deep appreciation go to Dr. Charles Tapalian and Dr. William Kelleher for making the Draper collaboration possible, and for the strong interest shown towards this project. Dr. Tapalian's scientific excellence and enterprise provided for a highly dynamic research effort and speedy progress.

I owe my gratitude to Dr. Brent Little for supplying vast amounts of ideas and guidance on theory and applications. Dr. Little's contributions were pivotal to the project.

Dr. Desmond Lim deserves the greatest recognition for his efforts in waveguide fabrication – and the greatest appreciation for being the best of friends. Vigorous thanks go to my friend Dr. Daniel Ripin for all the spirited discussions and scientific sparring that took place.

A heartfelt thank-you should be extended to all my friends in the U.S. and Europe who helped me along and who allowed me to get my mind off the work every now and then.

Finally, I would like to thank my parents, Eila and Jaakko, for their unwavering support over the years.

List of Publications

This dissertation is a review of the author's work in the field of high-Q resonator optics. It consists of an overview and the following selection of the author's publications in this field:

I

Surface-Roughness-Induced Contradirectional Coupling in Ring and Disk Resonators, B. E. Little, J. P. Laine and S. T. Chu, Optics Letters **22** (1997) 4-6.

II

Analytic Theory of Coupling from Tapered Fibers and Half-Blocks into Microsphere Resonators, B. E. Little, J. P. Laine, and H. A. Haus, Journal of Lightwave Technology **17** (1999) 704-715.

III

Etch-Eroded Fiber Coupler for Whispering-Gallery-Mode Excitation in High-Q Silica Microspheres, J. P. Laine, B. E. Little, and H. A. Haus, IEEE Photonics Technology Letters **11** (1999) 1429-1430.

IV

Pedestal Antiresonant Reflecting Waveguides for Robust Coupling to Microsphere Resonators and for Microphotonic Circuits, B. E. Little, J. P. Laine, D. R. Lim, H. A. Haus, L. C. Kimerling, and S. T. Chu, Optics Letters **25** (2000) 73-75.

V

Microsphere Resonator Mode Characterization by Pedestal Anti-Resonant Reflecting Waveguide Coupler, J. P. Laine, B. E. Little, D. R. Lim, H. C. Tapalian, L. C. Kimerling, and H. A. Haus, IEEE Photonics Technology Letters **12** (2000) 1004-1006.

VI

Planar Integrated Wavelength-Drop Device Based on Pedestal Antiresonant Reflecting Waveguides and High-Q Silica Microspheres, J. P. Laine, B. E. Little, D. R. Lim, H. C. Tapalian, and L. C. Kimerling, and H. A. Haus, Optics Letters **25** (2000) 1636-1638.

VII

Acceleration Sensor Based on High-Q Optical Microsphere Resonator and Pedestal Antiresonant Reflecting Waveguide Coupler, J. P. Laine, H. C. Tapalian, B. E. Little, and H. A. Haus, Sensors and Actuators A **93** (2001) 1-7.

Throughout this overview, these publications are referred to by their Roman numerals.

Author's Contribution

The research reported in this doctoral thesis has been carried out in the Research Laboratory of Electronics, Massachusetts Institute of Technology, and at the Charles Stark Draper Laboratory, mainly over the period 1998-2001.

The author has contributed extensively to all aspects of the research work presented in this thesis. All experiments reported in the Papers were set up and performed either entirely or to a very large extent by the author – including the initial creation of microsphere fabrication and integrated optics test facilities. The author performed most of the theoretical calculations, programming, and numerical computations in Papers I, III, V and VI, and he had an active role in such operations in Papers II, IV and VII. The author wrote Papers III, V, VI, and VII, and participated in the writing of Paper I, II, and IV. A body of results related to these papers has been presented by the author and co-authors at international conferences as well as in publications not included in this thesis[†].

[†] Examples of other presentations by the authors, related to the research area of the thesis:
- Tapalian, Laine, Lane, IEEE Photon.Technol. Lett. **14** (2002) 1118.
- OSA Integrated Photonics Research conf: Santa Barbara (1999), Quebec City (2000).
- Little, Chu, Haus, Foresi, Laine, J. Lightwave Technol. **15** (1997) 998.

Contents

1 Introduction

In 1912 Lord Rayleigh published "*The Problem of the Whispering Gallery*" [1], in which he considers sound waves traveling efficiently along the inside wall of an ovally shaped structure. His interest in this subject was raised by the phenomenon of being able to hear hushed voices and whispers over great distances in a domed cathedral: If the sound source and the listener were appropriately positioned, the dome could function as an exclusive acoustic conduit between the two – thus the term "whispering gallery".

The optical variety of the Whispering-Gallery Mode (WGM) is typically associated with circular-path resonant cavities [2]. Essentially, light inserted into an optical WGM travels exclusively via total internal reflection, glancing off material interfaces at near-parallel angle.

In recent years, research interest in optical WGM resonators has grown dramatically. This is due to the perception of great potential in optical communications signal processing applications. The component technologies in question involve mostly integrated waveguide-based rings and disks which are microfabricated onto wafer substrates using traditional integrated-circuit deposition and etching methods [3]. Ring-waveguide cavities have been envisioned in the roles of channel-dropping filters, switches, and even add-drop multiplexers. In the broad description, components based on the integrated WGM resonator should eventually defeat traditional fiber- and free-space optical counterparts through sheer economies-of-scale: functional ring-based components are typically very small in size compared with competing technologies, and the wafer-based fabrication processes are intrinsically oriented toward mass-manufacturing efficiency [4].

An intriguing micro-optical WGM resonator type, the solid-state microsphere, was introduced comparatively recently (for example, see [5]). The device was initially conceived as an improvement to microdroplet-based experimentation [6, 7], potentially permitting lasing and QED work in stable solid cavities. However, it was quickly recognized that the utility of the microsphere extended well beyond cavity-QED to include unique applications

in areas as varied as detection and sensing, high resolution spectroscopy, and even optical communications.

Specifically, microspheres are three-dimensional WGM resonators, a few hundred micrometers in diameter, often fabricated by simply melting the tip of an optical fiber. The total optical loss experienced by a WGM in such resonators can be extremely low – quality factors (Q) as high as 10^8-10^{10} are routinely demonstrated [8]. These extraordinary Q-values translate directly to high energy density, narrow resonant-wavelength lines and a lengthy cavity ringdown.

The WGM structure exhibited in a microsphere differs considerably from that of the planar waveguide ring resonator. Distinctively, the spherical cavity can support very complicated modes with equatorial, radial, as well as polar field dependencies [9]. Furthermore, the interpretation of the WGMs becomes significantly more elaborate if the resonator is deformed from the perfect spherical shape. Such diversity in modal structure can create special opportunities, as in the spherical wavelength-drop filter device described in Paper VI.

In many potential microsphere applications, the concept of operation often involves monitoring the parameters of the high-Q WGM resonance lines for signs of minute perturbations in the optical field. Since the quality factors are very high, even small scattering, coupling, or absorption out of the whispering-gallery mode set can be detected. In this thesis, this is best demonstrated by the acceleration sensor presented in Paper VII.

Until recently, the greatest impediment to the practical introduction of microsphere applications has been the difficulty of accessing the high-Q cavity. Efficient coupling has been accomplished only with the use of fragile, large, or otherwise impractical devices, such as bulk prisms or thin tapered fibers. However, a recent innovation, the stripline pedestal anti-resonant reflecting optical waveguide (SPARROW) coupler, is viewed as a very promising technology. See Paper IV.

This thesis consists of published studies in the field of optical microsphere WGM resonators, near-field couplers, and resonator applications.

Chapter 2 discusses the WGM mode structure as well as the exceptional energy-storage capacity of silica microspheres. Chapter 3 gives an overview of silica sphere fabrication. Chapter 4 considers various techniques of coupling light into the spherical resonators, and Chapter 5 consists of the application work performed during this thesis research.

2 Microsphere WGM Theoretical Framework

The very narrow optical resonance lines evident in solid-state microsphere or liquid microdroplet cavity experimentation are characteristic of whispering-gallery modes [10]. Light confined in such modes propagates by grazing-angle total internal reflection, circling the spherical particle in a thin and narrow band close to the surface. An individual WGM can be identified in terms of three mode numbers (n, m, l) which together represent the radial, equatorial, and polar electromagnetic field components. The radial part of a sphere WGM can be described by spherical Bessel functions with an external evanescent tail, while the polar – longitudinal – field dependence follows spherical harmonics, and the equatorial – latitudinal – field variation is sinusoidal [9], see Paper II. Specifically, n (= 1,2,...) gives the number of maxima in the radial field pattern of a particular WGM, while l (= 0,1,...) and m (= $-l$,...,0,...,l) help define the equatorial and polar field extent, see Figure 1, and Papers II and V [5,11,12,13,14]. Modes of highest field confinement correspond to high values of l, and opposite values of m correspond to waves propagating in opposite directions along the sphere equator. $l-|m|+1$ equals the number of lobes in the polar field.

Within a perfect sphere form, the resonant wavelength of any given WGM is determined only by l and n, since different radial and/or equatorial mode components correspond to different distances light must travel in order to complete a resonant path around the sphere. In this perfect-sphere case, the polar component in WGMs does not influence the resonant wavelengths. This degeneracy condition exists because field extension in the polar direction is countered exactly by a reduced optical path due to lesser circumference at higher latitudes. Importantly, if the perfect sphere is deformed into a spheroidal prolate or oblate shape, the polar degeneracy condition will be lifted and distinct polar resonances will be supported.

This chapter begins with a discussion on the origins of the high quality factors evident in silica microsphere WGM resonators, which is followed by a presentation of a theoretical framework for the silica microsphere WGM mode

structure. Finally, a formulation is presented linking spheroidal eccentricity to polar mode resonances in imperfect spheres (deformed spheroids).

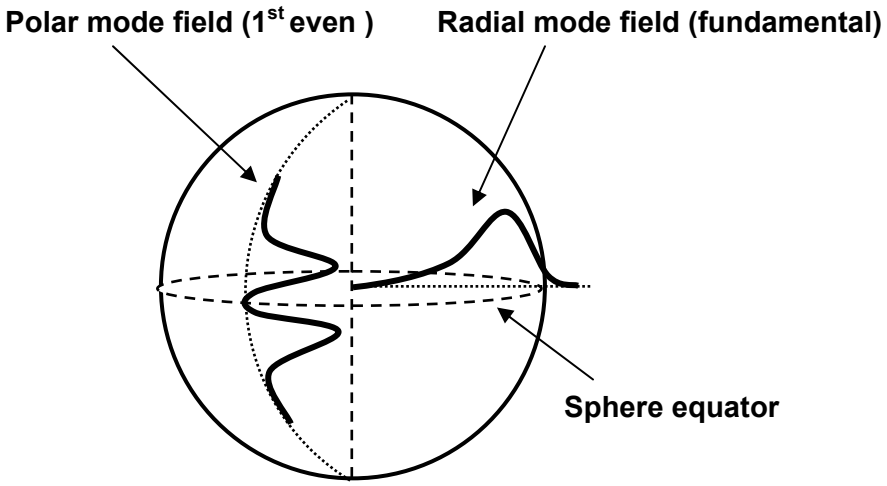

Figure 1: Schematic of WGM field components in a microsphere resonator (not to scale). Light trapped in the WGM propagates around the sphere equator in a narrow and thin band, constantly reflecting off the sphere surface at glancing incidence.

The radial field can be described by spherical Bessel functions inside the sphere and an exponential tail outside, while the polar component follows spherical harmonics, and the equatorial behavior is sinusoidal. A given WGM is identified by mode numbers *n, m,* and *l*. The value of *n* gives the number of maxima in the radial component, and $l-|m|+1$ gives the maxima in the polar component. Polar modes are often referred to as even or odd based on number of lobes.

2.1 Energy Storage

The performance of a resonator element is usually described in terms of its capacity to store energy. Obviously, such a capacity is constrained by processes that dissipate energy from the resonator. These loss processes can be classified into internal (attenuation, leakage, and scattering) and external (coupling). The storage capacities and loss effects of various resonator types

are quantified comparatively in Q, the mode quality factor for the resonator [10].

In an optical microsphere WGM resonator, energy storage may be thought of as the retention of individual light rays that have been inserted into the cavity [15]. Here, the value of the quality factor roughly equals the number of times a given ray can be expected to travel around the sphere before succumbing to a loss process. This total Q-value is composed of the intrinsic and coupling components – along the lines of the particular loss processes. In silica microspheres, internal loss effects include scattering from surface irregularities, absorption due to molecular resonances, Rayleigh scattering, and whispering-gallery tunneling. Surface scattering is usually relatively low, since the melting-based fabrication procedure creates an extremely smooth surface for the sphere. Tunneling losses become prominent only for sphere diameters of less than 30 μm (air-clad). Therefore, absorption and Rayleigh scattering dominate the losses. In terms of Q, the intrinsic factor within silica microspheres in the 1550 nm wavelength range is absorption-limited at approximately 10^{11}, assuming a water-free atmosphere [8,11]. Experimental efforts can easily produce Q-values up to 10^8, see Paper IV.

Such enormous Q-values are several orders of magnitude higher than those of other comparatively sized optical resonant cavities. As an example, the intrinsic Q in the closely related integrated-optics ring resonator component can be severely limited by surface roughness due to the required wafer-process etching steps [16], see Paper I. In Paper I, the specific case of loss-of-resonant power into a growing counterpropagating mode is studied. A formalism is developed to explain the resultant resonance splitting. It is important to note here that Paper I has been added to this thesis solely in order to give the reader a direct reference to the ring resonator and its loss processes – and the discussion further in the thesis will concentrate on the spherical resonators. Approximate comparative cavity performance characteristics are given in Table I. The high Q in the microspheres translates to narrow linewidths, long decay times, and high optical intensity.

Table I: Comparison of ring and sphere resonator intrinsic Q values in the 1550 nm wavelength range. Theoretical absorption limit for silica microspheres given in the last column.

	Best rings, disks	Standard sphere	Sphere limit
	$Q = 10^{3-5}$	$Q = 10^{7-8}$	$Q = 10^{11}$
Resonant linewidth:	GHz	MHz	kHz
Decay time:	ps	ns	μs
Decay length:	mm	m	km

2.2 Perfect Dielectric Sphere

WGM-trapped light traveling around a perfect sphere can be thought of as "zig-zagging" along an equator. The mode is confined to a belt around the equatorial plane by the curvature of the sphere in the polar direction. Different values of mode constant *m* define the amplitude of the zig-zag and thus the polar extent of the field. The mode propagation constant along this path is given by the projection of the wavevector $\boldsymbol{k}$ onto the surface of the sphere, the magnitude of which is

$$\beta_l = \sqrt{l(l+1)}/R \,,$$

in which R is the radius of the sphere. Assuming a planar surface, the projection of $\boldsymbol{\beta_l}$ onto the equator approximately equals

$$\beta_m = m/R \,.$$

Both $\boldsymbol{\beta_l}$ and $\boldsymbol{\beta_m}$ are parallel to the surface.

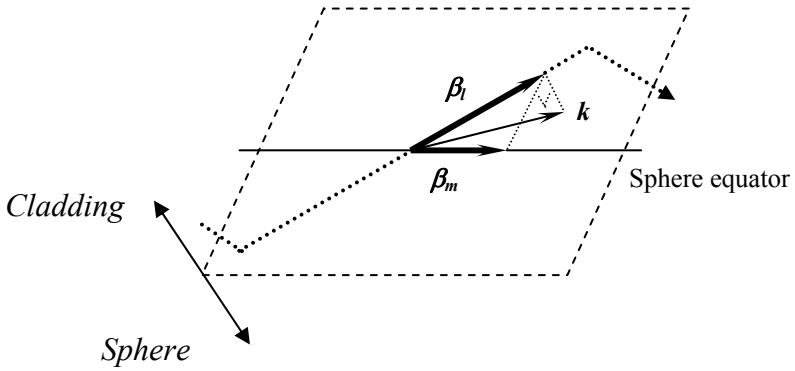

Figure 2: Vector schematic for $\boldsymbol{\beta}_m$, $\boldsymbol{\beta}_l$ and $\boldsymbol{k}$, relative to the sphere surface and to a notional mode path projection.

Obviously, the sphere only resonates at discrete values of the propagation constants. We create a characteristic equation connecting the resonances and mode numbers l and n of a perfectly spherical dielectric volume (Paper II):

$$\left(\eta\alpha + \frac{l}{R}\right) j_l\left(kn_s R\right) = kn_s j_{l+1}\left(kn_s R\right),$$

where

$$\alpha = \sqrt{\beta_l^2 - k^2 n_0^2}\ , k = 2\pi/\lambda\ ,$$

j_l and j_{l+1} are spherical Bessel functions, and η equals 1 for the TE polarization mode family and $(n_s/n_0)^2$ for TM (n_0 is the cladding index).

An initial guess for l is $l=kn_sR$. It is derived from the approximation that β_l is nearly equal to l/R, and that being a projection of $\boldsymbol{k}$, $\boldsymbol{\beta}_l$ will be of only slightly smaller magnitude than the $\boldsymbol{k}$ vector – especially in the limits of a fundamental mode and a large sphere size compared to the wavelength.

2.3 Deformed Sphere

A prolate or oblate deformation of the perfect sphere shape results in the lifting of polar WGM degeneracy. Now, the amplitude of the polar "zig-zagging" becomes meaningful as the sphere curvature no longer compensates the optical path length within modes digressing from the equator toward the poles. In other words, different values of *m* now represent distinct resonant wavelengths and the separation between these wavelengths corresponds to the degree of the spheroidal deformation.

In the following, an approach is discussed for linking the degree of polar-mode wavelength-splitting to spheroidal eccentricity, and to a particular polar mode number. In short, the variational principle is used to estimate the effects of small perturbations on the shape of a perfect sphere. Calculations are greatly simplified by substituting a metal-coated sphere for the silica sphere – thus removing one boundary-value problem from consideration. The resulting variational expression can then be used in conjunction with the characteristic equation of the dielectric sphere in order to pull together the wavelength-splitting, mode numbers, and the eccentricity of the sphere.

As in [17], the variational expression for the propagation constant *k* of an arbitrary waveguide with metallic boundaries is

$$k^2 = \frac{\int_V |\nabla \times E|^2 \, dV}{\int_V |E|^2 \, dV}.$$

A slight perturbation in the surface of the waveguide separates this expression into a sum of the original perfect boundary and the perturbation Δk

$$\frac{\int_V |\nabla \times E|^2 \, dV}{\int_V |E|^2 \, dV} + \frac{\int_{\Delta V} |\nabla \times E|^2 \, dV}{\int_V |E|^2 \, dV} = (k + \Delta k)^2 .$$

Since the perturbation is very small, $(k+\Delta k)^2$ roughly equals $k^2+2k\Delta k$, and thus

$$\Delta k = \frac{1}{2k}\frac{\int_{\Delta V}\left|\nabla \times E\right|^2 dV}{\int_V \left|E\right|^2 dV}.$$

In a spherical WGM resonator much larger than the wavelength, the electric fields are oriented either predominantly parallel or perpendicular to the surface of the sphere. In the case of a parallel electric field – a roughly TE-polarized orientation – the transversal field component is given by

$$E_\theta = \psi_{l-m}\sqrt{m}\theta j_l(kr)e^{-jm\phi},$$

where r, θ (polar angle), and ϕ are the spherical cordinates, and j_l is a spherical Bessel function of order l. Due to typically very small polar angles and high values of l and m (>500) at high-Q WGMs, ψ_{l-m} can be represented by Hermite-Gaussian functions [18]. The number of field maxima in the polar direction is l-m+1. For a fixed mode number l, modes with different m are degenerate in a perfect sphere (either metallic or dielectric). The eigenvalues in k are determined by the boundary condition that the field must vanish over the surface of the sphere. Since the transversal field component is significantly larger than the longitudinal one (by roughly a factor of m), this expression will function as the sole trial field for the variational expression.

Assuming a prolate or oblate spheroidal perturbation – i.e. the sphere is either flattened or elongated along the axis perpendicular to the propagation plane (equator), see Figure 3 – the perturbed spheroid boundary along the polar coordinate near the equator would follow roughly the expression

$$R(\theta) = R + \Delta R\theta^2,$$

where ΔR is the change in radius. After substitution and processing the variational expression, we finally get for the change in the wavevector k

$$\Delta k = \left(l - m + \tfrac{1}{2}\right)\frac{\Delta R}{R^2}.$$

For two consecutive polar modes $\Delta(l\text{-}m)$=1, we first find $\Delta k_{split} = \Delta R / R^2$, and then finally for the wavelength difference

$$\Delta\lambda \approx -\frac{\lambda^2}{2\pi}\frac{\Delta R}{R^2}.$$

The polar-mode resonant wavelength split is now directly related to the prolate or oblate eccentricity of the sphere.

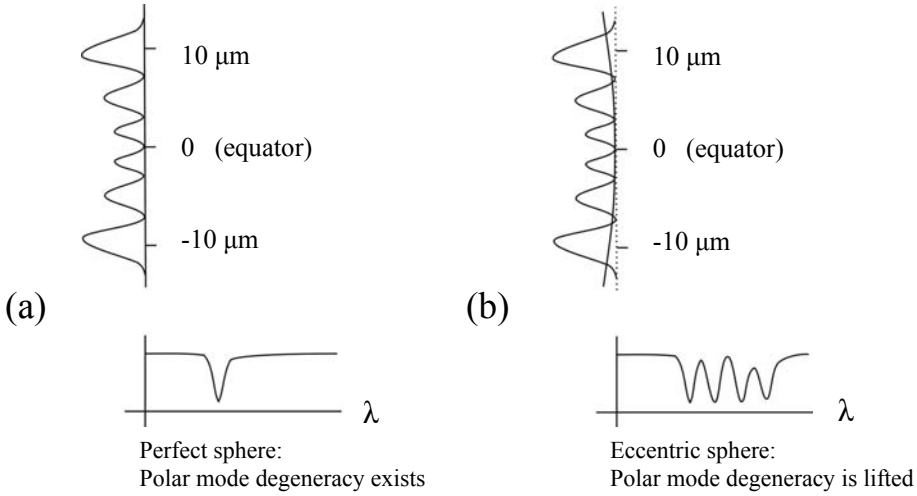

Figure 3: Resonant wavelength splitting of polar modes. In a perfect sphere (a) all polar WGM modes, such as the six-lobe (*m*=*l*-5) mode field cross-section illustrated beneath the surface of a 280 μm sphere, travel a common total optical path length, irrespective of the polar field extent of any particular mode. Therefore, in perfect spheres, a degeneracy condition exists for the polar mode components, with corresponding resonances falling on a common wavelength.

However, in the case of an eccentric sphere, as depicted in (b), the total path length of a WGM depends on the polar extent of the mode – leading to a spacing in the resonant wavelengths of the successive polar modes. The lifting of degeneracy can thus be utilized to find the eccentricity of the sphere by measuring the shift in the resonance frequencies of the modes. (Note that the equivalents of the TE/TM mode families for a dielectric sphere become degenerate in the metallic case.)

If required for mode identification purposes, the perturbed-sphere variational expression may be linked to the characteristic equation developed for the perfect dielectric sphere by matching it to an equivalent metallized sphere radius. This is performed by extracting the Goos-Hänschen shift from the total-internal-reflection angle-of-incidence that corresponds to a particular WGM.

Since $\boldsymbol{\beta_l}$ is the vertical projection of the wavevector $\boldsymbol{k}$ on the sphere surface, the angle of incidence experienced by a particular WGM can be calculated directly from the magnitudes of $\boldsymbol{\beta_l}$ and $\boldsymbol{k}$,

$$\Omega = arcsin\left(\frac{\beta_l}{kn_s}\right).$$

The Goos-Hänschen shift for an equivalent metallized sphere is then found by matching the field magnitudes and first derivatives of the radial standing-wave component and its exponential tail.

A simulating internal electric field is given by, for example [18] (a planar approximation is sufficient for sphere diameters roughly >100 μm at 1550 nm wavelength. Note: for clarity, the coordinate parameters here are different from those previously employed),

$$E(x,z) = e^{-j\gamma}\, 2E_{incident}\, cos(k_z z - \gamma) e^{-jk_x x} \ ,$$

in which

$$\gamma = -\tfrac{1}{2} arg\left(\left(\frac{j}{\tau} - \frac{1}{k_z}\right) \Big/ \left(\frac{j}{\tau} + \frac{1}{k_z}\right)\right) \quad , \quad k_z = kn_s\, cos(\Omega).$$

The exponential decay, with constant τ, is

$$E(x,z) = E_{through} e^{-\tau} e^{-jk_x x} \ .$$

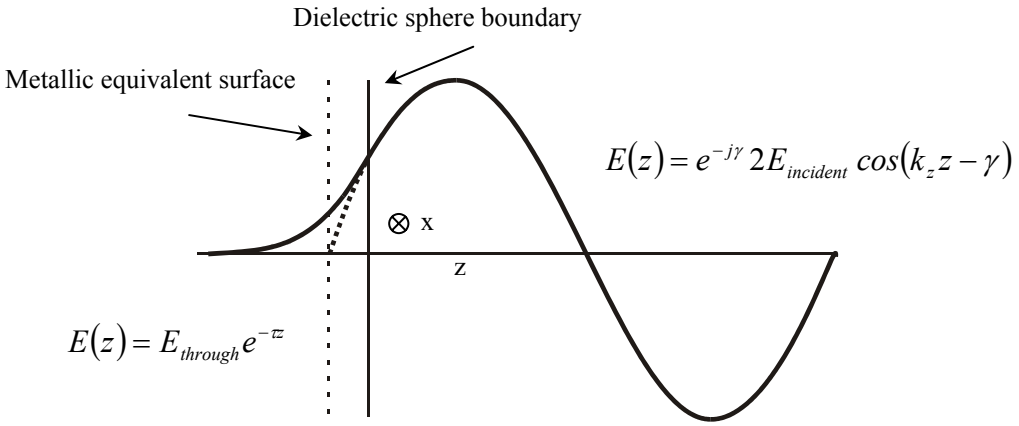

Figure 4: Utilizing the Goos-Hänschen shift. The general dielectric sphere case can be reduced to the simpler metallic-boundary environment.

2.4 Computed Wavelength Splitting

Applying the analysis to a notional dielectric sphere, we plot the calculated polar-mode wavelength split for five different *l*-numbers, see Figure 5. In an experimental setting, the preferable method for obtaining an initial guess for the mode number *l* is to fit a complete polar mode field pattern, Paper V; at 1.55 μm wavelength for a sphere diameter of 200-400 μm, the modes with best coupling efficiency are found between *l*=800 and *l*=1000.

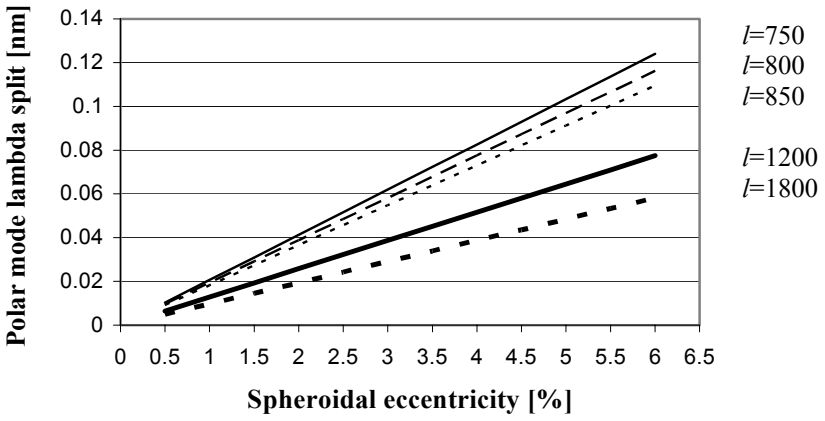

Figure 5: Calculated values of resonant wavelength splitting for successive polar modes in a prolate spheroid fall on the curves traced for *l*=750,…,1800 (*n*=1, *m*≈*l*, TE-equivalent, in the 1550 nm region). The diameter of the sphere is 280 μm.

We then proceed to the analysis of experimental wavelength-scan data. Figure 6 is a resonance plot of an approximately 280 μm diameter sphere. The pattern (dips A,B,C,D) is locally isolated and thus portrays a succession of degeneracy-lifted polar modes. The measured wavelength of the fundamental-mode resonance dip (A) is, in the limit of instrument accuracy: 1550.20 nm. The spacing between the successive polar-mode resonances is approximately 0.050 nm.

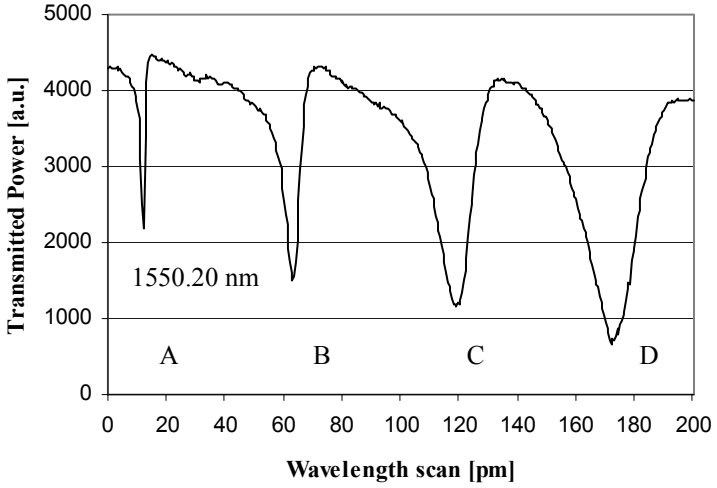

Figure 6: Experimental TE-data plot of microsphere whispering-gallery-mode resonances. The diameter of the sphere is 280 μm. First resonance-dip position (A) measured by a wavelength meter at 1550.20 nm.

Due to coupling parameters, Paper V, we assume best coupling at fundamental TE-resonance n=1. Performing experimental fitting for $\Delta(l\text{-}|m|)$=3,4 we have roughly l=800-900. The splitting then corresponds to a spheroidal eccentricity of roughly 2.5-2.8 % (ΔR < 10 μm). This constitutes a complete extraction of sphere and mode parameters from the given wavelength-scan data.

The precision of the method depends on the quality of the experimental data. Potentially significant imperfections in a spherical WGM-resonator experiment include: inaccuracy in the determination of the resonant wavelengths of the sphere (non-linear laser wavelength scan and/or wavelength metrology not sufficiently sensitive), incorrect assumptions on the physical parameters of the sphere (sphere size, shape, surface perturbations, local refractive index), unintelligible resonant and/or leakage processes (optical structure is more complex than a simple spheroid, and thus supports optical

processes other than those accounted for within the existing model), and finally, experimental reproducibility.

The above-listed unique error sources are difficult to address individually. First, the combined effect of the errors makes the task of isolating a particular error component quite problematic. Second, direct scrutiny of the error sources is limited by the accuracy and compatibility of measurement tools (wavelength meters, index profilers, interferometric profilometers, etc.). During the course of this work, it became evident to the authors that the correct approach to addressing the experimental error problem is to introduce extremely rigid guidelines for sphere fabrication and handling. In effect, a statistical improvement in sphere commonality partially offsets the need for interpreting individual sphere characteristics, and, on the other hand, simplifies the process of identifying the error sources.

In summary of this section, a formalism that directly links all the microsphere whispering-gallery mode numbers to the physical parameters of a sphere has been demonstrated. Perturbation theory is utilized to access the eccentricity of the spheroidal geometry. Calculations are simplified by substituting a metal-coated sphere for the dielectric. It is found that the method is accurate to within limits of comparative measurement.

In the first instance this tool can be used in the design of a general microsphere cavity experiment, for the purpose of determining the performance of a sphere of particular optical shape factor, and vice versa. Advanced applications include the design of wavelength switching elements, in which a tunable spherical cavity steers very narrow-band signals among the output ports. Another example is the multi-sample microsphere spectrometer, which can access different bands of a sphere's surface as a function of the particular mode number in use. Outside of the microsphere realm, the formalism could find use in the design of spheroidal low-grazing-angle mirror surfaces.

3 High-Q Microsphere Resonator Fabrication

The work presented in this thesis centers on the solid-state, silica microsphere cavity. Solid-state spheres have raised interest as practical WGM resonators partly because of a possibility to complement difficult liquid-droplet WGM cavity experiments. Also, silica automatically enjoys good compatibility with standard fiber-optics characterization instrumentation. Finally, achieving a high resonator quality level during fabrication is relatively straightforward with any standard silica source materials.

In this chapter, the fabrication of silica spheres is discussed, with a view of current individual sphere fabrication and a look at potential wafer-level manufacturing.

3.1 Microsphere Fabrication

Silica spheres can be fabricated by melting the end of an appropriately thin silica wire or post. In most cases, a stripped and cleaved length of inexpensive optical fiber, such as SMF-28, will work very well – producing spheres with a diameter of roughly above 150 μm. To achieve smaller diameters, a fiber can be thinned by tapering or etching.

The melting of the silica post is usually performed by electric arc or hydrogen flame heating. Both techniques have been found to produce a minimal amount of soot that attaches to the surface of the sphere and can spoil the low-loss cavity. Electric arcing is frequently carried out with fiber splicing equipment, which allows for exact positioning and energy transfer – resulting in reproducible sphere shapes and sizes. In this work, the majority of spheres were created via electric arc melting.

During fabrication, once the silica temperature passes the melting point, surface tension shapes the material into a spheroidal form. If the heat source is removed, solidification occurs instantaneously. It is possible to influence the sphere shape during fabrication by, for example, rotating the sphere or by increasing the molten mass of the sphere. If the deformation is drastic, the

spheroid particle diameter may differ significantly from the local curvature diameter at the effective WGM region (equator).

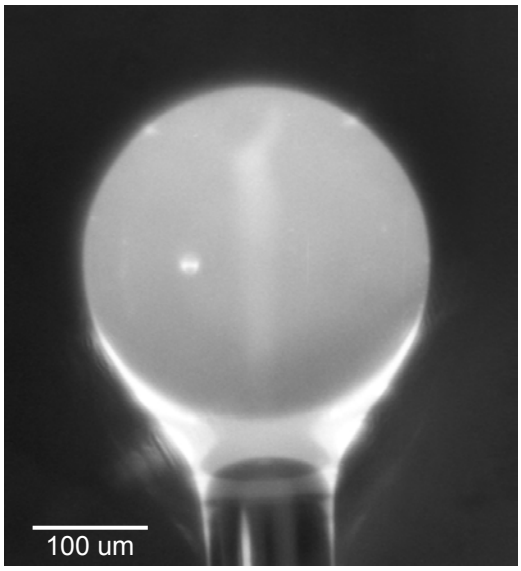

Figure 7: Fabrication of a silica microsphere resonator (electric arc heating). High-temperature silica glows as an opaque molten globe. Fiber stem is visible just beneath the globe.

After the fabrication stage, a microsphere destined for cavity experimentation does not necessarily require any further processing. However, if the sphere is to be coated with functional layers [19], it must pass through several additional steps, including: rigorous cleaning, plasma activation, application of the coating, and curing. For very-high-Q applications, the entire process of microsphere fabrication and packaging may be performed in an inert atmosphere, in order to eliminate contamination and water adsorption.

The characterization of finished microspheres typically involves optical measurements determining the attributes of the cavity (coupling efficiencies, resonance linewidths), as well as physical observations on sphere size, shape, and surface quality.

3.2 Wafer-Based Fabrication Technologies

Microsphere resonators could be manufactured commercially with the help of standard wafer processing technologies routinely used for the fabrication of integrated circuits and, to a lesser extent, optical waveguides [4]. The concept is to create structures on a silicon wafer that can then be molten into spherical form. Various permutations are possible, but a straightforward choice would be to create silicon posts topped with silica blocks, see Figure 8.

The driving forces for developing the wafer-based fabrication concept are: increased sphere-production rates, low cost, improved quality, and greater shape/size parameter commonality among the fabricated spheres. Additionally, such integrated platforms can ease the application of sphere technology in fields such as detection and sensing instrumentation, see Chapter 5.

Since the diameter of the wafer-fabricated sphere depends on the volume of the etched silica block, an important limiting factor in wafer-based sphere fabrication would be the maximum layer-deposition thickness that can be achieved with standard deposition techniques such as chemical vapor deposition [20,21], flame hydrolysis [22-24], or wafer oxidation [25-27].

In the most simple form of wafer-based sphere fabrication, a silicon wafer first undergoes oxidization to create a silica layer into the wafer. The wafer is then etched deep below the oxide layer base, while masking small rectangular or circular areas. During the etching, these masked areas leave small posts behind (consisting of a silicon base and a silica top). Finally, the wafer is exposed to controlled heating, so that the silica blocks develop spheroidal curvature while remaining attached to the silicon posts.

For comparison, in standard flame hydrolysis deposition, gaseous silane spray is heated to a high temperature and the resulting soot is deposited on a target wafer. This wafer is then placed into a furnace where the thick and porous soot is consolidated into a dense silica-glass layer. At this point the wafer and layers would be ready for sphere-post patterning and the final thermal sphere formation step, just as in the oxidized-wafer case.

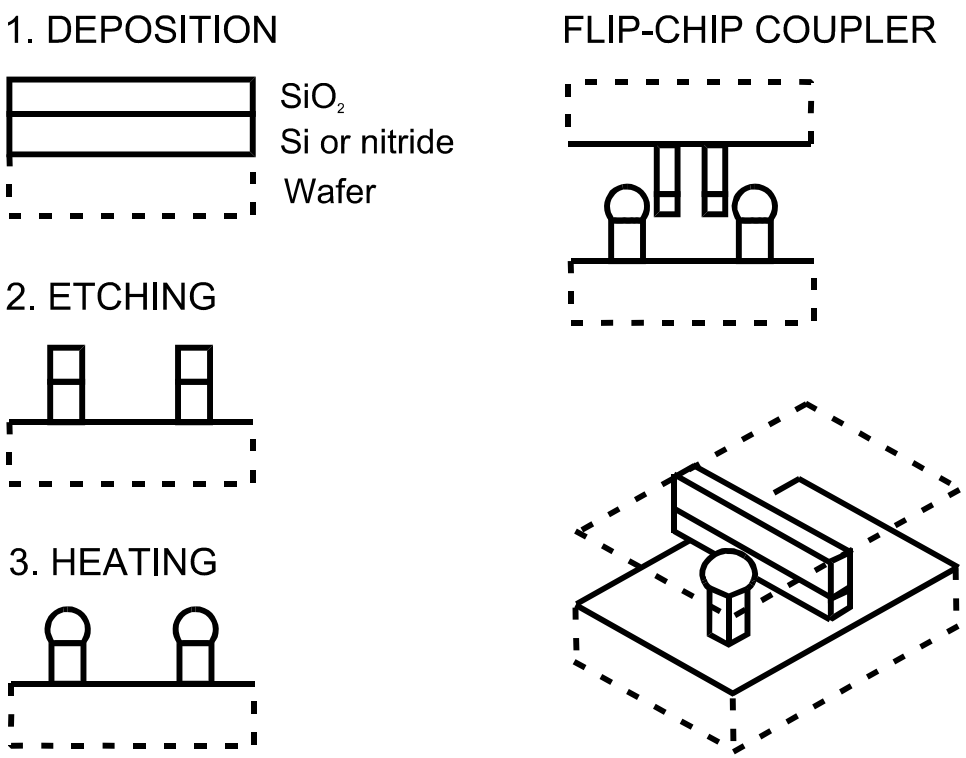

Figure 8: Silica microsphere fabrication with the help of semiconductor wafer manufacturing processes (also routinely used in optical waveguide fabrication). The spheres are formed on top of small posts by heating the entire wafer to the silica melting point. Optical access to the resonators is gained, for example, by a flip-chip bonded waveguide coupler component.

4 Optical Couplers

A significant challenge in utilizing high-Q narrow-linewidth optical resonators is the need to excite resonant modes efficiently while, simultaneously, making sure that the Q is not compromised. In the case of the microsphere, this implies that along with maintaining a sphere surface clean of perturbations and contaminants that would attenuate or scatter light out of the resonant modes, one must control external factors affecting the Q as well. Here, interest focuses principally on the performance of the device with which light is passed into and out of the sphere: the coupler.

The ideal microsphere WGM coupling device includes the following characteristics: (A) efficient WGM excitation performance with little potential for Q-spoiling, (B) simple sphere-to-coupler alignment, (C) clearly defined ports, (D) robust and integrable structure, and (E) a consistent and inexpensive fabrication process.

Requirement (A) – efficient coupling – can be achieved with a variety of evanescent-field techniques ranging from bulk prisms to fiber tapers [5,10,28-33], see Figure 9. In these techniques, an exponentially decaying optical field at the coupler's glass-air interface functions to transfer power from the coupler into the whispering-gallery modes of the sphere. The efficiency of a given evanescent coupler type is determined primarily by the overlap of the sphere and coupler mode fields and the matching of mode propagation constants. Yet other factors, such as the length of the coupling region, can play significant roles as well, see Paper II and Chapter 2. Importantly, if the light trapped in the sphere modes finds alternate paths to escape back into the coupler structure (for example, into the cladding), the resonator system will experience unexpected Q-spoiling and a lower total efficiency. To circumvent such phenomena, coupler designs should isolate the sphere modes from the cladding and other superstructure.

Adding requirements (B) and (C) – ease-of-alignment and discrete ports – narrows the field of evanescent-field couplers to purely guided wave devices. To illustrate: in bulk prism couplers, the positions of all components (light source, prism and sphere) must be carefully adjusted in order to reach the

optimal coupling conditions. Furthermore, the readout of sphere resonances has to be performed either by observation of scattered light from the sphere or by collecting light from the prism. In contrast, a typical tapered-fiber guided-wave coupler requires no elaborate spatial position optimization, and can be easily fitted with fiber-connectorized input and output ports.

Finally, robustness and good integrability (D), as well as fabrication concerns reflecting on device mass manufacturability (E), suggest an integrated, wafer-fabricated coupler design. It is possible that such unique couplers – based on optical waveguide elements created by standard integrated circuit fabrication methods – will become comparatively very inexpensive and thus competitive in the fielding of microsphere applications.

During the course of this thesis work, two new coupler types were developed: the etch-eroded fiber coupler, and the stripline pedestal anti-resonant reflecting optical waveguide coupler. These devices are discussed in the following sections, as well as in papers III and IV.

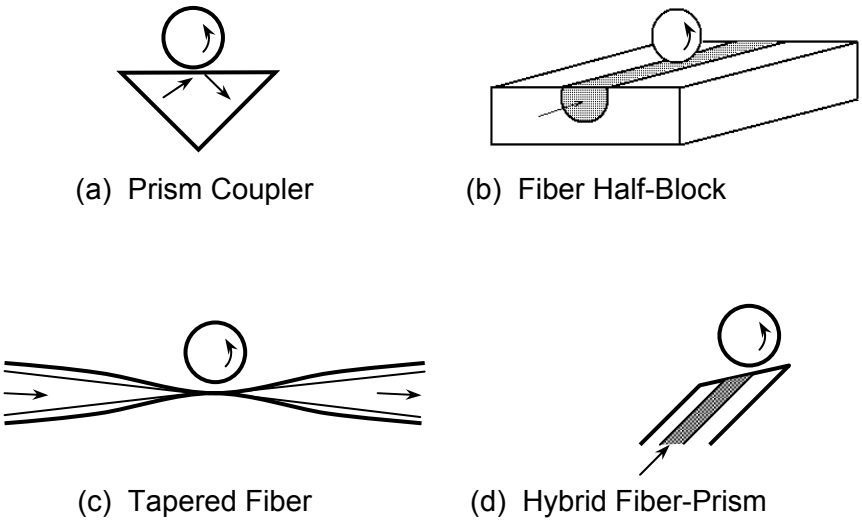

Figure 9: Examples of microsphere resonator whispering-gallery-mode couplers. All techniques presented here are based on transferring power via evanescent-field coupling.

(a) Prism-to-sphere coupling [28] is among the earliest concepts and requires only relatively inexpensive hardware. In this method, a laser beam is directed into a prism so as to achieve total internal reflection at the prism surface. This results in a tunneling optical field at the surface's glass-air interface, which is then used to couple light into the sphere resonator. However, achieving optimal alignment of system components is challenging.

(b) The fiber half-block [31] consists of an optical fiber buried in glass or wedged in a metal block. The fiber is polished to the core, thus allowing access to the optical mode. The most significant drawback of this technique is the leakage of light from sphere modes into the fiber cladding and into the surrounding block.

(c) The tapered fiber [29] is a very powerful coupling tool, since it allows sensitive tuning of the fiber-mode propagation constant by controlling the fiber thickness. Tapers are most commonly fabricated by heating and drawing (similar to preform fiber drawing), for example with the help of advanced fiber splicing equipment. A specific difficulty for taper couplers is that the tapered zone of the fiber is usually very thin (often less than 5 μm in diameter) and therefore very delicate.

(d) The fiber-prism [33] combines the advantages of waveguide light insertion with prism coupling. In this method, a fiber end is polished into an angled plane, which then acts as a total-internal-reflection surface for guided light from the fiber. Thus, the fiber-prism method eliminates most of the alignment steps that are necessary for bulk prism couplers.

4.1 Etched Fiber Coupler

The first novel coupler design developed in the course of this thesis work is the etch-eroded fiber coupler, see Fig. 10, described in Paper III. The operation principle is similar to the standard heat-and-pull tapered fiber coupler, i.e. access to the fiber mode is gained by exposing the evanescent field tail. The principal motivation for the etch-eroded fiber coupler lies in the low cost and simplicity of single-unit fabrication compared to other coupling methods.

The light-guiding layers of a representative 1550 nm wavelength-range single-mode optical fiber [34] consist of a cylindrical cladding surrounding a core rod – with a combined diameter of about 125 μm and a core diameter of 8-10 μm. The refractive index of the core is higher than that of the cladding (here by roughly 0.3-0.5%), which results in most of the fiber light being trapped in the core. Looking at a cross-section of the fiber, along a radial axis, the fundamental-mode field amplitude is a Bessel function within the core and decreases exponentially after passing the core-cladding interface. In conventional low-loss fibers, this field tail is protected from absorptive and scattering effects on or beyond the cladding's outer surface simply by setting a sufficient cladding thickness.

In side-coupling fiber coupler arrangements, the goal is to deliberately tap into the optical mode through this protective cladding barrier. The etching procedure proposed here can remove layers of the fiber material, controllably, in a hydrofluoric acid solution. The primary technical difference from the standard heat-and-draw tapering is that etch erosion actually reduces cladding thickness – while fiber drawing tapers both the core and the cladding (essentially combining them into a single rod). In addition, the etching procedure can create arbitrary-length homogeneously eroded regions, which allows "sphere wrap-around" (i.e. coupling-length control). An analytical treatment of tapered-fiber coupling can be found in Paper II.

In experimentation, sphere-mode coupling efficiencies of over 30% have been demonstrated.

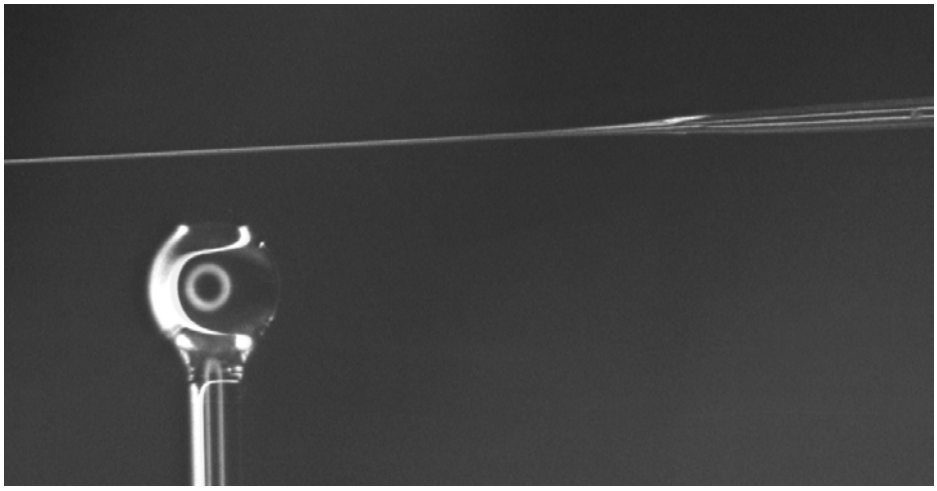

Figure 10: Etch-eroded fiber coupler (horizontal structure), with silica microsphere. Sphere diameter roughly 0.3 mm.

4.2 SPARROW Coupler

As outlined earlier in this chapter, it is recognized that a wafer-fabricated integrated coupler structure would be the preferable platform for practical microsphere applications and laboratory experiments as well. However, it is not until quite recently that such planar waveguide coupler technology has been successfully demonstrated, see Paper IV. The short explanation for this is that conventional surface waveguide structures have cladding materials of relatively low refractive index that roughly matches the index of the silica in high-Q microspheres. As a result, a silica sphere coupled to a conventional surface waveguide will lose most of its energy to the waveguide cladding and substrate. This loss lowers the Q and reduces device efficiency. The problem could be reduced if, for example, the waveguide cladding index were to be made significantly lower than that of the sphere silica. However, materials of a sufficiently low index are not available for modern waveguide fabrication technology. The SPARROW structure (Stripline Pedestal AntiResonant Reflecting Optical Waveguide) is designed to circumvent this problem, see Figure 11.

SPARROWs consist of a standard waveguide core fabricated on top of a vertically oriented high-reflection stack of alternating high- and low-index layers [35]. The thicknesses of the layers correspond to a quarter of the vertically directed guide-light wavelength. The function of this stack is to confine light into the core and isolate it from the rest of the structure as well as from the wafer. If the layering is fabricated correctly, a reflection better than 99% can be expected at the first interface. Guide core thickness and width are selected to provide an effective index compatible with the chosen sphere parameters.

In experimentation, coupling efficiencies of over 98%, and Q values of over 10^8, have been demonstrated.

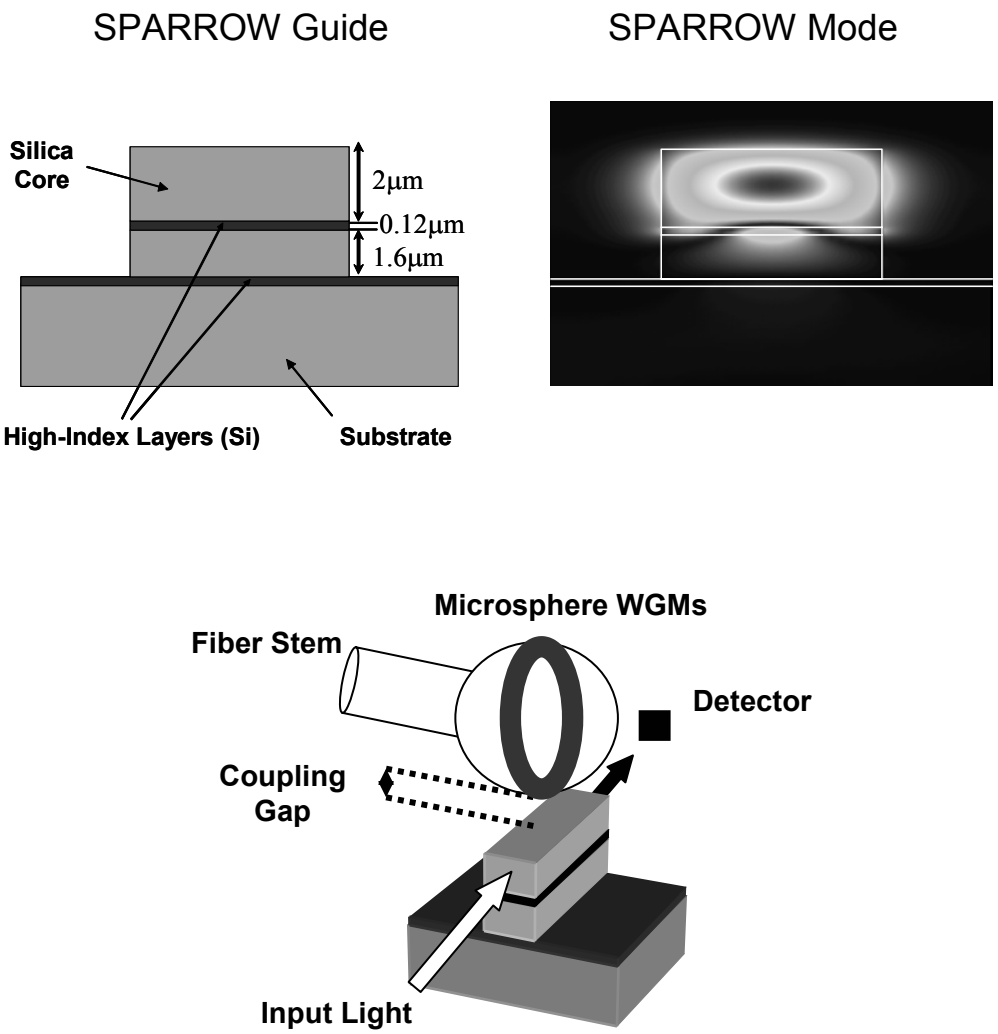

Figure 11: (Top) Example of a SPARROW guide structure and numerically computed mode field – wavelength 1550 nm, layer indexes: low 1.45, high 3.5, substrate 1.45. Note: The mode is strongly confined to the core, and calculated for silica substrate.

(Bottom) Schematic of microsphere resonator usage with SPARROW coupler.

5 Applications

The most familiar application areas of generic optical resonator constructions are found in laser cavities and resonant filters [3,36-39]. Advanced applications in optical communications, such as wavelength-selective attenuators and switches, are in the focus of current research. The miniature high-Q microsphere resonators considered in this thesis could potentially find use in such categories, for example in narrow-band switches. However, since the quality factors of the spheres are extremely high, they are very well suited for detection and sensing purposes as well. In this section, we consider two examples of functional application demonstrations for microsphere-based components, described in Papers VI and VII [40-44].

5.1 Wavelength-Drop Device

Paper VI presents an extremely narrow-band planar wavelength-drop device based on the integrated SPARROW coupler platform. In this concept, adjacent waveguides exchange power through the whispering-gallery modes of a microsphere.

Specifically, two SPARROW guide pedestals are employed for independent sphere input and output coupling. One guide extends across the length of the coupler substrate, providing ports for both optical power insertion and throughput detection. For a fiber-coupler analog, see [45]. The second guide originates at the midway point on the chip and operates exclusively as a drop port for the resonator. To complete the wavelength-drop arrangement, the microsphere is positioned above and between the two pedestals in such a way that the coupling parameters at resonance are optimized for power transfer from the input guide into the drop guide, see Figure 12.

In experimentation, transfer efficiencies higher than 50% were routinely observed in the range of 20-50 MHz linewidths.

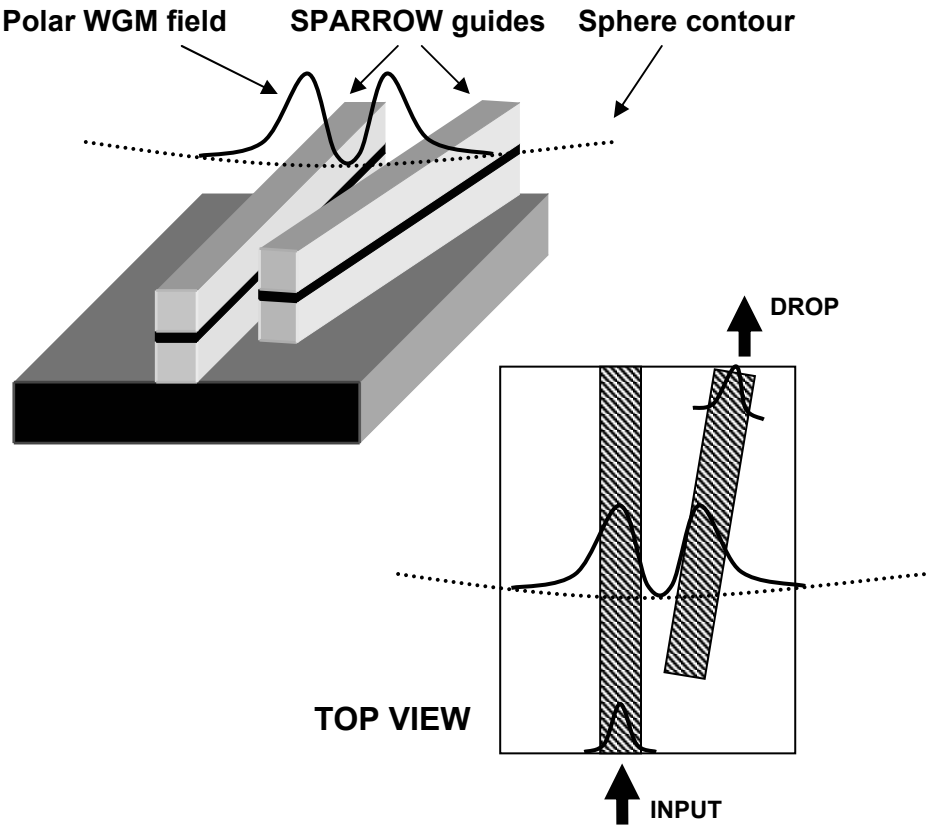

Figure 12: Schematic of the narrow-band planar wavelength-drop device. Power is transferred from a SPARROW input guide into the drop guide via the whispering-gallery modes of a microsphere resonator. The sphere is positioned above and between the two guides. Since the mode fields of the waveguides do not substantially overlap, there is very little direct coupling and, therefore, the sphere essentially fills the role of a wavelength-drop filter.

In the example rendered here, the field envelope of an even polar WGM component (two lobes) is overlaid on the guide-chip along with the sphere curvature contour (dotted line). Power transfer efficiency is primarily determined by losses experienced in the sphere and field overlap optimization between the sphere and guide modes.

5.2 Acceleration Sensor

In order to utilize microsphere WGM resonators in the sensor function, the given sensing task must be reduced to a measurement of perturbations in the sphere's optical state. The measurements are performed here via direct monitoring of resonance parameters: resonant-line wavelength, linewidth, and amplitude.

Perturbations can be brought about in the sphere system by either internal or external means. The most straightforward external method is to vary the coupling gap between the input coupler and the resonator [46,47]. Another example is to perturb the sphere WGM evanescent field with a probe. Internal means include changes in the optical path length due to sphere deformation or a change in the refractive index [12].

The acceleration sensing configuration presented in Paper VII is based on the coupling gap variation method. The device consists of a silica microsphere and a SPARROW coupler chip. Integration of the sphere and the coupler is accomplished by attaching the sphere's fiber stem to the dynamic system of the waveguide so that the sphere is suspended above the coupling waveguides, see Figure 13. The fiber stem acts as a flexure beam for the spherical resonator, responding to external forces influencing the dynamic system. A force applied along a vertical axis normal to the waveguide-element surface results in a sphere displacement relative to the waveguide.

Once such displacement occurs, the changing coupling parameters are directly reflected in resonance line width, wavelength, and amplitude. Specifically, as the coupling gap is reduced, an increase in both linewidth and amplitude is observed. However, once the sphere is moved very close to the coupler – into a region where the coupler dominates WGM losses (overcoupling) – the amplitude of the sphere resonances may in fact begin to decrease [29]. In addition, as the coupling gap continues to decrease, the coupler itself begins to act as a perturbation to the sphere mode field and a corresponding shift in resonance wavelength can be observed [48].

In the experimentation, light was coupled from a tunable 1550 nm diode laser into the SPARROW waveguide, from which the microsphere then extracted the WGM resonant wavelengths. The monitoring of sphere

movements was accomplished by constantly sweeping the laser line across a chosen microsphere resonance, accompanied by simultaneous translation of waveguide output intensity values into resonance parameter data. Finally, this data was processed to represent the acceleration experienced by the device. All computing was performed in real time – enabled by specially configured data-acquisition cards and signal-processing software.

During the experimental phase, a detection resolution of less than 1 mg and a noise floor of roughly 100 μg were demonstrated (1 mg ≈ 0.0098 m/s^2).

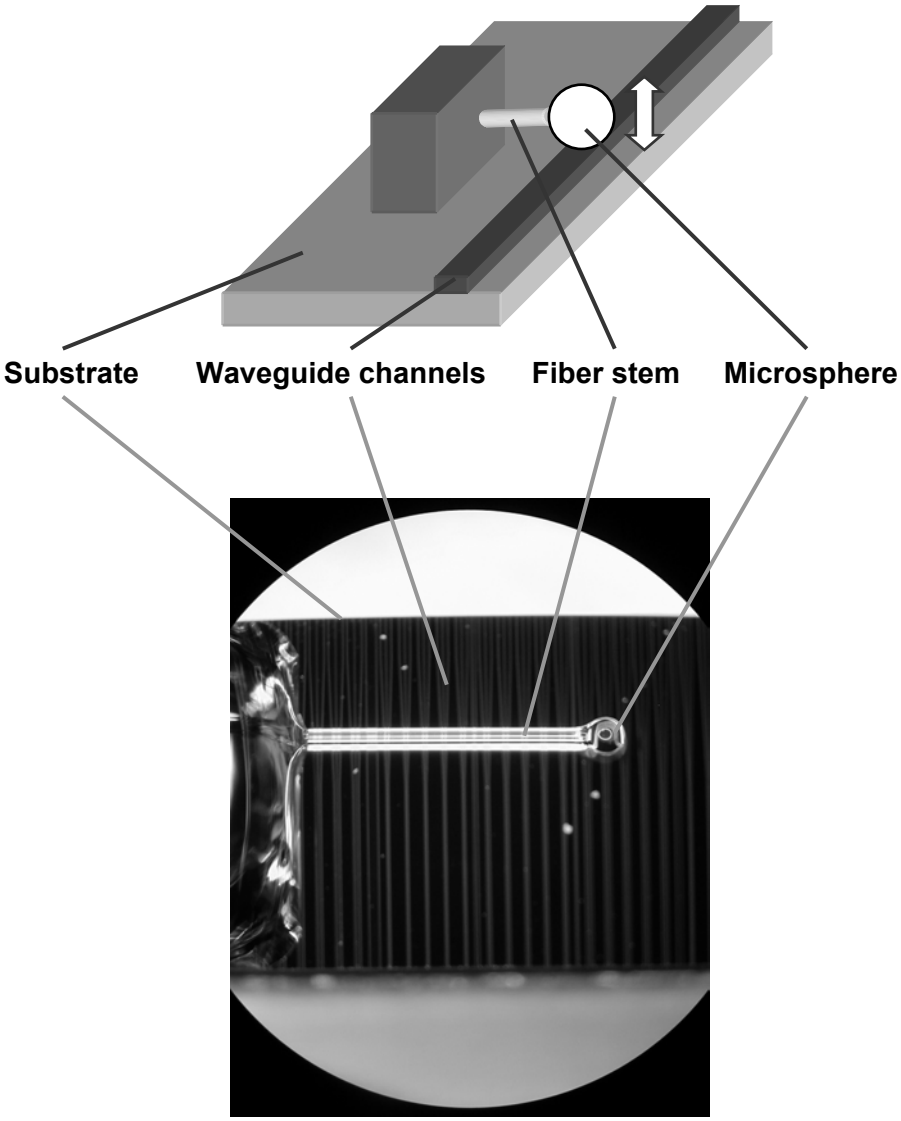

Figure 13: Schematic drawing and microscopic photograph of a microsphere-based acceleration sensing device. A single resonator is suspended above a SPARROW waveguide coupler chip. Sphere movements due to external forces acting on the device are registered as changes in the wavelength, linewidth, and amplitude of a sphere WGM resonance. Sphere diameter here is roughly 200 μm.

5.3 Functional Coatings – Environmental Sensing

At the end of this doctoral program, a significant research effort was launched in the area of microsphere-based environmental sensing. Although much of this work has not reached publication, nor is it described in the Papers forming this thesis, a very brief description of this work will give the reader a better appreciation for the range of applications available to the miniature, high-performance optical element. General references to environmental and medical sensing are given in: biological [49-58], chemical [59-69].

The underlying concept is to utilize the microsphere WGM resonator as a platform for advanced functional coatings that are capable of classifying atmospheric pathogens and chemical species [70-73]. In some cases, such coatings consist of a silane-originated base layer and a selection of "bucket molecules" either bonded to the top of the base layer or mixed into it. The base layer is designed to act as an anchor and an intermediary, adhering to the surface below while simultaneously hosting the actual functional material. The role of the functional bucket molecules is then to extract a given particulate species from the surrounding air stream, and hold it for long enough that a measurement confirming its presence can be performed.

In the absence of target particles, the effect of such coatings on an optical microsphere resonator's WGM modes is absorptive. The evanescent optical field is exposed to the coating, thus depleting energy from the mode primarily as a function of coating thickness. Additionally, partly dependent on the quality of coating adhesion, scattering effects may occur as well.

Once target particles are introduced into the sphere's environment and the bucket molecules begin to operate, the coating will simply accumulate the particle material. This fluctuation can be detected in several ways, the most common of which being a change in coating absorptivity, a resultant slight increase in optical loss and thus broadening of the resonant line.

In this work, all coatings were applied in a four-step process involving chemical cleaning, plasma cleaning and activation, coating, and curing.

6 Summary and Conclusions

In this thesis, research in silica microsphere optical whispering-gallery-mode resonators has been discussed. Resonator Q factors of over 10^8 have been demonstrated at roughly 1550 nm wavelength, corresponding to optical linewidths in the picometer scale. Such extremely high-Q characteristics could, in principle, create great interest for microsphere applications extending from novel detection and sensing tasks to cavity-QED experimentation. Until recently, however, significant difficulties have been encountered in gaining efficient access to the high-Q sphere modes. In this thesis, two new coupling tools have been presented to ease this task, the etch-eroded fiber and the SPARROW waveguide. The SPARROWs are fabricated in the standard integrated circuit wafer-manufacturing process and therefore have a robust integrable structure with accurate and reproducible dimensional parameters. In this thesis, SPARROW couplers have been shown to reach sphere-mode coupling efficiencies of over 95%.

Within the thesis work, a microsphere wavelength-drop device based on the SPARROW has been fabricated, demonstrating drop linewidths of less than 30 MHz. Also, a microsphere acceleration sensor has been built, with a detection resolution of <1 mg demonstrated experimentally. Finally, theoretical understanding of sphere modes and coupling has been developed during the project.

In the author's view, the thesis results show decisively that the microsphere high-Q resonator concept can indeed be harnessed into practical utility. With the basic optical coupling difficulties now essentially solved, interest begins to shift to other issues, such as consistent and inexpensive sphere fabrication, further device integration, and generally application-oriented innovation. Predicting the development on these tracks, it can be said with some confidence that budding planar technologies will likely allow wafer-scale production of microspheres. This could revolutionize both fabrication cost and quality consistency. A parallel effort in sphere-to-SPARROW integration, focusing on for example flip-chip technology derivatives, may yield a mechanism to connect the two optical elements into one monolithic unit. These

integrated platforms would allow the joining of the resonator function with various advanced waveguide optical functions, and even electronics – all within the same component. The goal of such high-level integration would be self-containment; ultimately combining source, detector, and processing.

The emerging platforms will, with high likelihood, advance especially sensor/detector development. This is surmised from the microsphere's implied excellence in the measurement role, i.e. a microsphere-based system would probably be slated to challenging sensing tasks and, thus, likely to be required to function as a stand-alone unit or as a solitary station of a distributed sensor network. In such a context, platform integration would be paramount.

In lieu of sensor efforts, other serious developmental paths will undoubtedly form. Clearly, for example, optical physics experimentation will continue to utilize the microsphere as a high-Q "intensity generator". Other examples include current laboratory work on microsphere-based lasers, oscillators, switches and filters. However, it is difficult to determine now which segments of such efforts, if any, will translate into more robust activity outside of the research community.

In the end, it should be noted that right now, the microsphere optical resonator is still, fundamentally, a creature bound to the university optics laboratory. It is fervently hoped, however, that the work outlined in this thesis could be the basis for an accelerated future.

References

[1] Lord Rayleigh, “The problem of the whispering gallery”, Scientific Papers (Cambridge University) **5** (1912) 617-620.

[2] E. A. J. Marcatili, “Bends in optical dielectric waveguides”, B.S.T.J. **48** (1969).

[3] B. E. Little *et al.*, “Microring resonator channel dropping filters”, J. Lightwave Technol. **15** (1997) 998-1005.

[4] D. Elliott, “Integrated circuit fabrication technology”, McGraw-Hill, New York, 1989.

[5] L. Collot *et al.*, “Very high-Q whispering-gallery mode resonances observed on fused silica microspheres”, Europhys. Lett. **23** (1993) 327-334.

[6] D. W. Vernooy *et al.*, “Cavity QED with high-Q whispering gallery modes”, Phys. Rev. A **57** (1998).

[7] R. K. Chang *et al.*, “Optical processes in microcavities”, Adv. Series in Appl. Phys. 3, World Scientific, Singapore, 1996.

[8] M. L. Gorodetsky *et al.*, “Optical microsphere resonators: optimal coupling and the ultimate Q”, SPIE **3267** (1998) 251-262.

[9] J. Stratton *et al.*, “Elliptic cylinder and spheroidal wave functions including tables of separation constants and coefficients”, Wiley, New York, 1941.

[10] V. B. Braginsky *et al.*, “Quality-factor and nonlinear properties of optical whispering-gallery modes”, Phys. Lett. A **137** (1989) 393-396.

[11] M. L. Gorodetsky *et al.*, “On the ultimate Q of optical microsphere resonators”, Opt. Lett. **21** (1996) 453-455.

[12] V. S. Ilchenko *et al.*, “Strain-tunable high-Q optical microsphere resonator”, Opt. Comm. **145** (1998) 86-90.

[13] A. Serpenguzel *et al.*, "Excitation of resonances of microspheres on an optical fiber", Opt. Lett. **20** (1995) 654-656.

[14] J. P. Laine *et al.*, "Novel techniques for WGM excitation in high-Q silica microspheres", Digest of Integrated Photonics Research conference, Opt. Soc. Am. (1999) 238-240.

[15] A. Mekis *et al.*, "Ray chaos and Q spoiling in lasing droplets", Phys. Rev. Lett. **75** (1995) 2682-2685.

[16] B. E. Little *et al.*, "Microring resonator arrays for VLSI photonics", IEEE Photonics Technol. Lett. **12** (2000) 323-325.

[17] K. Morishita *et al.*, "Unified approach to the derivation of variational expression for electromagnetic fields", IEEE Trans. Microwave Theory and Tech. **25** (1977) 34-40.

[18] H. A. Haus, "Waves and fields in optoelectronics", Prentice-Hall, New Jersey, 1984.

[19] H. C. Tapalian *et al.*, "Thermo-optical switches using coated microsphere resonators", IEEE Photonics Technol. Lett. **14** (2002) 1118-1120.

[20] O. Haiyan, "Different index-contrast silica-on-silicon waveguides by PECVD", Electronics Lett. **2** (2003) 212-213.

[21] H. Sato, "Preparation of a BaF/CaF slab optical waveguide by chemical vapor deposition", Japanese J. of Appl. Phys. **3A** (1994) 368-370.

[22] Y. Wu *et al.*, "Fabrication of planar optical waveguide material on silicon by flame hydrolysis deposition", SPIE **4580** (2001) 251-256.

[23] K. Schmidt *et al.*, "Building passive components with silica waveguides", SPIE **3795** (1999) 313-319.

[24] S. Blanco *et al.*, "Electron-beam-induced densification of Ge-doped flame hydrolysis silica for waveguide fabrication", Appl. Phys. Lett. **18** (2001) 2889-2891.

[25] T. Yuhai *et al.*, "Microscopic dynamics of silicon oxidation", Phys. Rev. Lett. **8** (2002).

[26] Z. Taofang *et al.*, "Growth of ultrathin silicon dioxide films during rapid-thermal oxidation", 9th Intl. Conf. on Advanced Thermal Processing of Semicon. (2001) 287-295.

[27] J. Ngau *et al.*, "Silicon orientation effects in the initial regime of wet oxidation", J. Electrochem. Soc. **8** (2002) 98-101.

[28] M. L. Gorodetsky *et al.*, "High-Q optical whispering-gallery microresonators: Precession approach for spherical mode analysis and emission patterns with prism couplers", Opt. Comm. **113** (1994) 133-143.

[29] J. C. Knight *et al.*, "Phase-matched excitation of whispering-gallery-mode resonances by a fiber taper", Opt. Lett. **22** (1997) 1129-1131.

[30] D. W. Vernooy *et al.*, "High-Q measurements of fused-silica microspheres in the infrared", Opt. Lett. **23** (1998) 247-249.

[31] N. Dubreuil *et al.*, "Eroded monomode optical fiber for whispering-gallery mode excitation in fused-silica microspheres", Opt. Lett. **20** (1995) 813-815.

[32] G. Griffel *et al.*, "Morphology-dependent resonances of a microsphere-optical fiber system", Opt. Lett. **21** (1996) 695-697.

[33] V. S. Ilchenko *et al.*, "Pigtailing the high-Q microsphere cavity: A simple fiber coupler for optical whispering-gallery modes", Opt. Lett. **24** (1999) 723-725.

[34] A. Snyder *et al.*, "Optical waveguide theory", Chapman & Hall, London, 1983.

[35] M. A. Duguay, "Antiresonant reflecting optical waveguides in silica-silicon multilayer structures", Appl. Phys. Lett. **49** (1986) 13-17.

[36] S. Chang *et al.*, "Stimulated emission and lasing in whispering-gallery modes of GaN microdisk cavities", Appl. Phys. Lett. **75** (1999) 166-168.

[37] S. McCall *et al.*, "Whispering-gallery mode microdisk lasers", Appl. Phys. Lett. **60** (1992) 289-291.

[38] Y. Hibino *et al.*, "Silica-based optical waveguide ring laser integrated with semiconductor laser amplifier on Si substrate", Electronics Lett. **20** (1992) 1932-1933.

[39] K. Iwatsuki *et al.*, "Waveguide-type optical passive ring-resonator gyro using time-division detection scheme", Electronics Lett. **25** (1989) 688-689.

[40] V. S. Ilchenko *et al.*, "Coupling and tunability of optical whispering-gallery modes: A basis for coordinate meter", Opt. Comm. **107** (1994) 41-48.

[41] F. Treussart *et al.*, "Quantized atom-field force at the surface of a microsphere", Opt. Lett. **19** (1994) 1651-1653.

[42] B. E. Little *et al.*, "Track-changing using the phase response of microspheres and resonators", Opt. Lett. **23** (1998) 894-896.

[43] S. Arnold *et al.*, "Room-temperature microparticle-based persistent spectral hole burning memory", Opt. Lett. **16** (1991) 420-422.

[44] V. Sandoghar *et al.*, "Very low threshold whispering-gallery mode microsphere laser", Phys. Rev. A. **54** (1996) 1777.

[45] C. Ming *et al.*, "Fiber-optic add-drop device based on a silica microsphere whispering-gallery mode system", IEEE Photonics Technol. Lett. **11** (1999) 686-687.

[46] A. Yariv, "Critical coupling and its control in optical waveguide-ring resonator systems", IEEE Photonics Technol. Lett. **14** (2002) 483-485.

[47] D. Marcuse, "Coupled mode theory of optical resonant cavities", J. of Quantum Electronics **21** (1985) 1819-1826.

[48] F. Treussart *et al.*, "Microlasers based on silica microspheres", Ann.Telecommun. **52**, pp.557-568, 1997.

[49] L. Bansal *et al.*, "Fiber-optic neurotoxin sensor", Bioengineering Conf. IEEE Proc. (2002) 221-222.

[50] S. Jeonggi *et al.*, "Biophotonic MEMS for single molecule detection and manipulation", Microtechnologies in Medicine and Biology 2nd Annual Conf. Proc. (2002) 363-368.

[51] T. Sulchek *et al.*, "Interdigital cantilever as a biological sensor", Nanotechnology Conf. IEEE Proc. (2001) 562-566.

[52] A. J. Berger, "Novel near-infrared Raman spectroscopy of biological fluids", Lasers and Electro-Optics Society LEOS Proc. (2001) 261-262.

[53] G. Durry, "In situ sensing of the atmosphere with telecommunication laser diodes", Lasers and Electro-Optics CLEO Tech. Digest (2001) 290-291.

[54] A. Fielding *et al.*, "Tapered single-mode optical fiber evanescent coupling", IEEE Photonics Technol. Lett. **14** (2002) 53-55.

[55] D. Jiang *et al.*, "Study on a new fiber-optic glucose biosensor", Optical Fiber Sensors Conf. Tech. Digest (2002) 451-454.

[56] K. Misiakos *et al.*, "Monolithic silicon optoelectronic biochips", Electron Devices Meeting IEDM Tech. Digest (2001).

[57] B. C. Gibson *et al.*, "Evanescent field analysis of air-silica waveguides (for biosensor applications)", Lasers and Electro-Optics Society LEOS Proc. (2001) 709-710.

[58] R. L. Smith *et al.*, "Photonic microinstruments for biomolecular sensing and analysis", Lasers and Electro-Optics Society LEOS Proc. (2001) 390-391.

[59] D. M. Wilson *et al.*, "Chemical sensors for portable, handheld field instruments", Sensors Journal **1** (2001) 256-274.

[60] H. P. Ho *et al.*, "A chemical sensor based on the measurement of differential phase related to surface plasmon resonance", Electron Devices Meeting Proc. (2001) 56-59.

[61] D. A. Cohen *et al.*, "A monolithic chemical sensor using tandem heterodyned sampled grating DBR lasers", Lasers and Electro-Optics Society LEOS Proc. (2001) 238-239.

[62] G. Lammel *et al.*, "MEMS infrared gas spectrometer based on porous silicon tunable filter", Micro Electro Mechanical Systems Conf. Proc. (2001) 578-581.

[63] Z. M. Qi *et al.*, "A composite optical waveguide-based polarimetric interferometer for chemical sensing applications", J. Lightwave Technol. **18** (2000) 1106-1110.

[64] F. Nikolajeff, "The use of micro-optics for miniaturized chemical and biomedical analysis systems", Optical MEMS Conf. Proc. (2000) 65-66.

[65] A. T. Rosenberger, "Whispering-gallery-mode evanescent-wave microsensor for trace-gas detection", Biomedical Instrumentation SPIE Proc. (2001).

[66] T. M. Butler *et al.*, "Integrated optical Bragg-grating-based chemical sensor on a curved input edge waveguide structure", Opt. Lett. **24** (1999) 525-527.

[67] K. A. Remley *et al.*, "Design and analysis of a silicon-based antiresonant reflecting optical waveguide chemical sensor", Opt. Lett. **21** (1996) 1241-1243.

[68] T. Lee *et al.*, "Chemical sensing with microbent optical fiber", Opt. Lett. **26** (2001) 1541-1543.

[69] S. Tao *et al.*, "Porous solgel fiber as a transducer for highly sensitive chemical sensing", Opt. Lett. **27** (2002) 1382-1384.

[70] W. Lukosz *et al.*, “Principles and sensitivities of integrated optical and surface plasmon sensors for direct affinity sensing and immunosensing”, Biosensors Bioelectronics **6** (1991) 215-225.

[71] G. Boisde *et al.*, “Chemical and biochemical sensing with optical fibers and waveguides”, Artech House, Boston, 1996.

[72] B. Swanson *et al.*, “Cyclodextrin-based microsensors for volatile organic compounds”, Polymers in Sensors: Theory and Practice, (Oxford University Press) (1998) 130-138.

[73] A. K. Ray, “Organic films for nanoelectronics and sensing applications”, Nanotechnology Proc. (2001) 540-543.

Abstracts of Publications I-VII

I

Reflections that are due to random surface roughness in periodic structures such as dielectric rings and disks inherently phase match forward- and backward-propagating modes. Small reflections are thus considerably enhanced and may impair the performance of traveling-wave resonators. In addition, such contradirectional coupling leads to a splitting of the resonant peak. These effects are studied analytically.

II

Coupling from tapered fibers and polished half-block couplers into the high-Q whispering-gallery modes of microsphere resonators is investigated analytically. Numerous formulas derived to predict the external coupling Q values, and intrinsic whispering-gallery loss, for arbitrary structures, and for any sphere mode. Phase mismatch due to the differences in propagation constants between input and sphere modes is taken into account. These formulas are strictly mechanical once a simple characteristic equation is solved which related the spherical mode orders to the resonant wave vector. Results are in very good agreement with values that are calculated by different numerical methods.

III

A simple and inexpensive technique for the excitation of whispering-gallery modes in silica microspheres is presented. In this technique, the cladding of a single-mode optical fiber is etched chemically in order to expose the fiber's evanescent field. The cladding can be eroded partially, or removed completely with continued etching into the core. The etch-erosion procedure requires a minimum of specialized equipment and preparation time.

IV

Strip-line pedestal antiresonant reflecting waveguides are high-confinement, silica integrated optical waveguides in which the optical modes are completely isolated from the substrate by thin high-index layers. These waveguides are particularly well suited for whispering-gallery mode excitation in high-Q microspheres. They can also be used in microphotonic circuits, such as for microring resonators. The theory and design of these structures are highlighted. Experiments that show high coupling efficiency to microspheres are also demonstrated.

V

The stripline pedestal anti-resonant reflecting optical waveguide (SPARROW) is an efficient and robust coupling device for silica microsphere whispering-gallery-mode excitation. The concept incorporates alternating layers of Si and SiO_2, designed to isolate the mode of the sphere and the waveguide from the dielectric substrate. Experimental charaacterizations of this coupling technique are presented, including displacement measurement, and whispering-gallery-mode intensity mapping. Power extraction efficiencies of over 98% are reported.

VI

Whispering-gallery modes in silica microspheres can be accessed very efficiently with the recently introduced stripline pedestal antiresonant reflecting optical waveguide (SPARROW) structure. This integrated-optics coupling technique creates novel application opportunities for the high-Q spherical cavities. We report the demonstration of a narrow-band wavelength-drop configuration utilizing SPARROW waveguides and a silica microsphere.

VII

A novel acceleration sensing concept utilizing high-Q microsphere whispering-gallery mode resonators is presented. Induced flexure-arm displacements are monitored through changes in the resonance characteristics of a spherical optical cavity coupled to the flexure. Instantaneous measurement sensitivity of better than 1 mg at 250 Hz bandwidth, and a noise floor of 100 μg are demonstrated.

ISBN 951-22-6447-1
ISSN 1456-3320